Thermal–Mechanical and Spectroscopic Analysis of Fast-growing Tropical Hardwoods *Paraserianthes falcataria* and *Neolamarckia cadamba*

Norzarish Qistina Mohd Yusli,[a] Yosafat A. Pranata,[b] Ong Chee Beng,[c] Johari Zainudin,[d] Nur Ilya Farhana Md Noh,[e] and Zakiah Ahmad [a,*]

Thermo-mechanical and chemical behaviour of two tropical plantation timbers, Batai (*Paraserianthes falcataria*) and Laran (*Neolamarckia cadamba*), were investigated using dynamic mechanical analysis (DMA) and Fourier transform infrared spectroscopy (FTIR). The DMA was conducted with a heating rate of 2 °C/min at frequencies of 1, 2, and 5 Hz. The results revealed frequency- and species-dependent differences in storage modulus (*E′*), loss modulus (*E″*), and damping factor (tan *δ*) across 25 to 250 °C. Batai exhibited lower stiffness but higher damping capacity, with sharper tan *δ* peaks corresponding to hemicellulose relaxations, whereas Laran demonstrated higher stiffness, broader transitions, and reduced damping due to its lignin-rich matrix. The glass transition temperature (T_g) determined from tan *δ* peaks was more distinct for Batai (95 to 102 °C) than Laran (83 to 126 °C), confirming contrasting relaxation behaviours. The FTIR spectra further distinguished the species: Batai showed sharper carbohydrate-associated peaks, indicating more crystalline cellulose domains, while Laran displayed stronger hydroxyl, carbonyl, and aromatic absorbance linked to hemicellulose and lignin. Correlating DMA and FTIR findings highlighted that Batai's greater damping arises from its accessible amorphous domains, while Laran's enhanced stiffness stems from its crosslinked lignin–hemicellulose network.

DOI: 10.15376/biores.21.2.3115-3136

Keywords: Batai (Paraserianthes falcataria); Laran (Neolamarckia cadamba); DMA; FTIR; Glass transition temperature; Viscoelasticity; Thermal degradation; Tropical plantation timber; Stiffness; Damping

Contact information: a: Faculty of Civil Engineering, Universiti Teknologi Mara, 40450, Shah Alam, Selangor, Malaysia; b: Master Program in Civil Engineering, Maranatha Christian University, Jl. Suria Sumantri 65, Bandung, 40164, West Java, Indonesia; c: Forest Research Institute Malaysia (FRIM), 68100 Kuala Lumpur, Malaysia; d: Sarawak Timber Industry Development Corporation, 93050 Kuching, Sarawak, Malaysia; e: Faculty of Civil Engineering, Universiti Teknologi Mara, 40450, Shah Alam;
**Corresponding author: zakiah@uitm.edu.my*

INTRODUCTION

Wood has emerged as a key renewable material in sustainable construction. It offers favourable strength-to-weight ratios, carbon sequestration capacity, and aesthetic value. However, its application in fire-sensitive structures remains limited by uncertainties in its thermal degradation and fire resistance. The fire performance is governed by a complex interaction between thermal exposure, mechanical degradation, combustion processes, and char formation, all of which evolve progressively with increasing temperature. When

exposed to elevated temperatures, wood undergoes complex thermo-chemical transformations: cellulose depolymerises, hemicellulose softens and decomposes, and lignin undergoes gradual cross-linking and breakdown. These processes collectively determine stiffness retention, dimensional stability, charring rate, and ultimately the load-bearing capacity of timber during fire exposure. A molecular-to-mechanics understanding of these transitions is therefore essential for improving predictive fire models and developing modified woods and composites with enhanced fire performance.

As a thermally thick and anisotropic material, timber develops pronounced temperature gradients across its cross-section when subjected to fire or elevated heat flux, resulting in spatially varying mechanical and thermo-physical responses. These gradients play a critical role in controlling both fire susceptibility during the early stages of heating and structural integrity during prolonged fire exposure (White and Dietenberger 2010; Lee and Park 2022).

Mechanical degradation of wood begins at relatively low temperatures, with reductions in stiffness and strength reported at temperatures as low as 60 to 70 °C due to the softening of cell-wall polymers (White and Dietenberger 2001; Moraes *et al.* 2005). As temperature increases to around 100 °C, moisture evaporation dominates the heat transfer process, leading to a temporary temperature plateau associated with the latent heat of vaporisation. This stage delays further temperature rise but contributes to internal stress redistribution and microstructural damage (Bartlett *et al.* 2019; Junior *et al.* 2024).

At higher temperatures, typically between 200 and 225 °C, timber undergoes pyrolysis, releasing combustible volatiles and initiating char formation (Wong *et al.* 2017; Žajdlík and Šuhajda 2022; Meena *et al.* 2023). The subsequent growth of the char layer reduces the effective load-bearing cross-section while simultaneously acting as a thermal barrier that limits heat penetration into the unburnt core. The rate of char formation and the stability of the char layer are therefore critical parameters controlling combustion severity, mass loss, and fire resistance.

Characterising mechanical degradation using Dynamic Mechanical Analysis (DMA) prior to ignition and during early pyrolysis provides a valuable link between material-scale thermo-mechanical behaviour and fire-scale processes such as combustion development and char formation (Kutnar *et al.* 2013; Bartlett *et al.* 2019). DMA is a thermo-mechanical technique in which an oscillatory force is applied to a specimen, and the resulting deformation is recorded and analysed to provide information on the material's viscoelastic behaviour. DMA is a widely used technique to monitor the viscoelastic behaviour of polymers and composites across temperature and frequency domains. DMA enables simultaneous assessment of stiffness (modulus), which reflects the material's ability to store elastic energy, and damping (viscosity), which represents its ability to dissipate energy as heat due to internal friction (Menard and Menard 2015).

The fundamental outputs of DMA are the storage modulus (E'), describing the elastic response or energy storage; the loss modulus (E''), describing the viscous response or energy dissipation; and the loss factor ($\tan \delta = E''/E'$), a measure of damping and the overall balance between elasticity and viscosity (Havimo 2009). These three parameters together provide a comprehensive picture of viscoelasticity and all of which are sensitive to thermal softening and degradation of the amorphous polymer phases.

When a specimen is subjected to a temperature sweep, DMA can detect molecular relaxations associated with polymer chain mobility and changes in free volume. A significant peak or shift in $\tan \delta$ often signals a transition, such as the glass transition temperature (T_g), which marks the transition from a glassy, rigid state to a more rubbery,

ductile state (Ferry 1980; Menard and Menard 2015). Such transitions are critical in polymers and polymer-based composites, as they directly affect stiffness, damping, and thermal stability.

As wood is itself a composite material consisting of the three main natural polymers, cellulose, hemicellulose, and lignin, its viscoelastic properties can also be characterised using DMA. Species-dependent differences are particularly evident in viscoelastic behaviour, arising from variations in both the proportion and chemical structure of hemicelluloses and lignin across different woods. Classic work by Pettersen (1984) established that hardwoods and softwoods differ significantly in their polysaccharide and lignin composition, with hardwoods generally containing more xylans (O-acetyl-4-O-methylglucuronoxylans) and syringyl-rich lignins, while softwoods are dominated by mannans (galactoglucomannans) and guaiacyl lignins. These compositional contrasts directly influence relaxation behaviour detected by DMA: hemicelluloses, being amorphous and hygroscopic, govern low- to mid-temperature transitions through their susceptibility to softening and plasticisation by moisture (Olsson and Salmén 2004), whereas lignin contributes to broader, higher-temperature relaxations due to its aromatic network and degree of cross-linking (Backman and Lindberg 2001). Recent studies further highlight how these chemical distinctions modulate wood's response under thermal and fire conditions. For instance, Kutnar *et al.* (2021) demonstrated that thermo-hydro-mechanically treated beech, with its S-rich lignin, exhibited a pronounced shift in tan δ and stiffness reduction, whereas spruce showed a more gradual decline. Horiyama *et al.* (2023) confirmed that intra-annual ring variations in lignin and hemicellulose distribution also produce micro-scale differences in viscoelasticity, underscoring the multi-level influence of species chemistry. Studies have shown that relaxations associated with hemicellulose and lignin appear between 80 to 200 °C, coinciding with the onset of fire-induced weakening (Salmén 1984; Sun *et al.* 2007; Kutnar *et al.* 2021). As fire conditions accelerate thermal decomposition, DMA offers a means of quantifying the progressive mechanical loss that underpins structural failure in heated timber.

Fourier Transform Infrared Spectroscopy (FTIR) provides complementary chemical information by tracking functional groups associated with cellulose, hemicellulose, and lignin. Bands associated with hydroxyl stretching (≈ 3300 cm^{-1}), carbonyl groups (≈ 1720 cm^{-1}), aromatic lignin vibrations (≈1600 to 1510 cm^{-1}), and carbohydrate fingerprints (≈ 1200 to 900 cm^{-1}) shift in intensity or position as wood polymers degrade (Poletto *et al.* 2012; Traoré *et al.* 2018; Fellak *et al.* 2022). These spectral signatures reveal hemicellulose deacetylation, lignin condensation, and cellulose crystallinity loss—all processes directly tied to mechanical relaxation and charring.

While DMA captures how wood loses stiffness and dissipates energy under heating, FTIR explains why, by linking these macroscopic changes to polymer-level transformations. Integrated DMA–FTIR analysis therefore provides a powerful framework for fire performance research: correlating modulus loss with hemicellulose deacetylation, or damping peaks with lignin aromatic transitions, for example, enables mechanistic attribution. This combined approach has been applied successfully in biomass pyrolysis and polymer degradation studies (Liu *et al.* 2008; Apaydın Varol and Mutlu 2023), but remains underutilised in the context of wood fire resistance especially for tropical timbers.

The aim of this study is to integrate DMA and FTIR to elucidate the thermo-mechanical and spectroscopic behaviour of selected tropical plantation woods under heating. Through correlating viscoelastic relaxations with chemical degradation signatures, this study seeks to (i) quantify thermo-viscoelastic responses (E', E'', tan δ, apparent T_g) in

identifying critical temperature ranges for stiffness and damping loss (ii) identify temperature-dependent chemical signatures (O–H, C=O, aromatic lignin, polysaccharide fingerprints); and (iii) establish cross-property correlations that explain species-specific stiffness, damping, and thermal stability.

The temperature-dependent changes in viscoelastic properties obtained from DMA, together with chemical transformations identified by FTIR, provide a strong basis for predicting ignition behaviour, heat release, smoke generation, and char formation. If one combines DMA and FITR with cone calorimeter testing, a clear relationship can be established between changes in mechanical properties, chemical structure, and fire reaction behaviour, since cone calorimeter test shows how it actually burns under fire exposure. When correlating DMA and FTIR with cone calorimeter data, it is possible to link changes in storage modulus, damping behaviour, and FTIR-identified chemical functional groups to key fire reaction parameters such as time to ignition, peak heat release rate, mass loss rate, smoke production, and carbon monoxide (CO) yield.

Such a multi-scale approach would enable more mechanistic interpretation of flammability behaviour and support the development of predictive fire-performance models for wood products, contributing to improved fire-resistant design and material screening methodologies.

EXPERIMENTAL

Materials

This study utilised two tropical plantation timber species, Batai (*Paraserianthes falcataria*) and Laran (*Neolamarckia cadamba*), sourced from Sabah. The materials were supplied as solid timber blocks that were free from visible defects, including knots, cracks, or decay, and were in a dry condition. These species were chosen for investigation due to their ready availability as fast-growing plantation timbers in Malaysia and their growing significance for structural and industrial applications. The DMA specimens were cut from three different blocks per species that were air dried. The nominal specimen dimensions were width of 12 mm (radial), length of 60 mm (longitudinal), and a thickness of 6 mm (tangential). For FTIR specimens, the wood block for both species were manually chipped into smaller fragments (Fig. 1a) and then ground into fine particles using a high-speed mechanical grinder (Fig. 1b).

Fig. 1. Preparation of wood particles: (a) manual chipping, (b) grinding into fine particles, and (c) sieving through 250-um mesh to achieve uniform particle size

The wood particles were sieved through a 250-µm mesh to obtain a uniform particle size (Fig. 1c). Approximately 5 mg of the sieved wood particles were used for each FTIR measurement.

Figure 2 shows the prepared wood particles. These particles were stored in sealed containers under dry conditions prior to FTIR analyses.

(a) (b)

Fig. 2. Prepared wood particles: (a) Batai and (b) Laran

Test Methods

The dynamic mechanical properties of the wood samples were measured using a TA Instruments DMA Q800 (TA Instruments, New Castle, DE, USA) equipped with a three-point bending clamp (Fig. 3a). Rectangular specimens were measured for length, width, and thickness using a digital caliper and weighed prior to testing. The specimens were then positioned horizontally on the two supports and secured at the centre loading point of the three-point bending clamp (Fig. 3b).

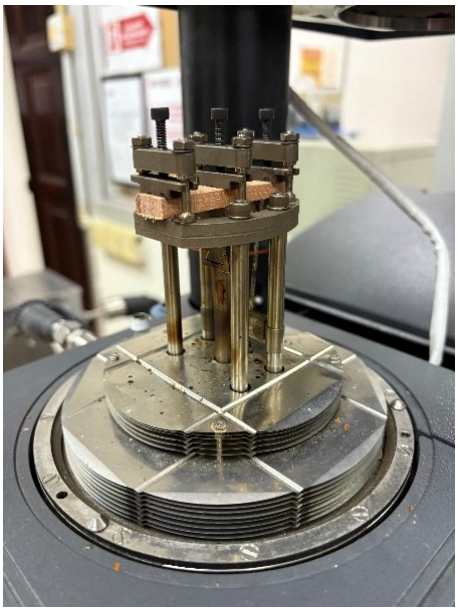

Fig. 3. Specimen clamped in a TA Instruments DMA Q800 using three-point bending setup

The test was performed in temperature-sweep mode from 25 to 250 °C at a heating rate of 2°C/min. A sinusoidal oscillatory load was applied at 1, 2, and 5 Hz. The storage modulus (E'), loss modulus (E''), and damping factor (tan δ) were continuously recorded

as functions of temperature. The DMA data were analysed to identify thermal transitions and to evaluate the viscoelastic behaviour of the two timber species.

Fourier Transform Infrared (FTIR) spectroscopy was conducted to identify the functional groups and major chemical constituents in Batai and Laran wood particles. The analysis was carried out using a Perkin Elmer Spectrum 400 FTIR spectrometer (Perkin Elmer Inc., Hillsboro, OR, USA) in Attenuated Total Reflectance (ATR) mode. Approximately 5 mg of each wood sample were placed directly onto the ATR crystal without any chemical treatment or pre-conditioning, and the spectra were collected over the range of 4000 to 400 cm^{-1}. The FTIR data were interpreted based on the presence and intensity of characteristic absorbance bands associated with cellulose, hemicellulose, lignin, and other functional groups inherent in the wood matrix.

RESULTS AND DISCUSSION

Dynamic Mechanical Analysis

The dynamic mechanical analysis (DMA) trends for Batai and Laran were found to be consistent with viscoelastic theory for wood, which identifies three principal stages; glassy, transition (viscoelastic), and rubbery. These stages correspond to the thermal and moisture-dependent responses of its main constituents: cellulose, hemicellulose, and lignin. The curve for storage modulus for Batai at 1 Hz is used as an example to explain the general characteristics as shown in Fig. 4.

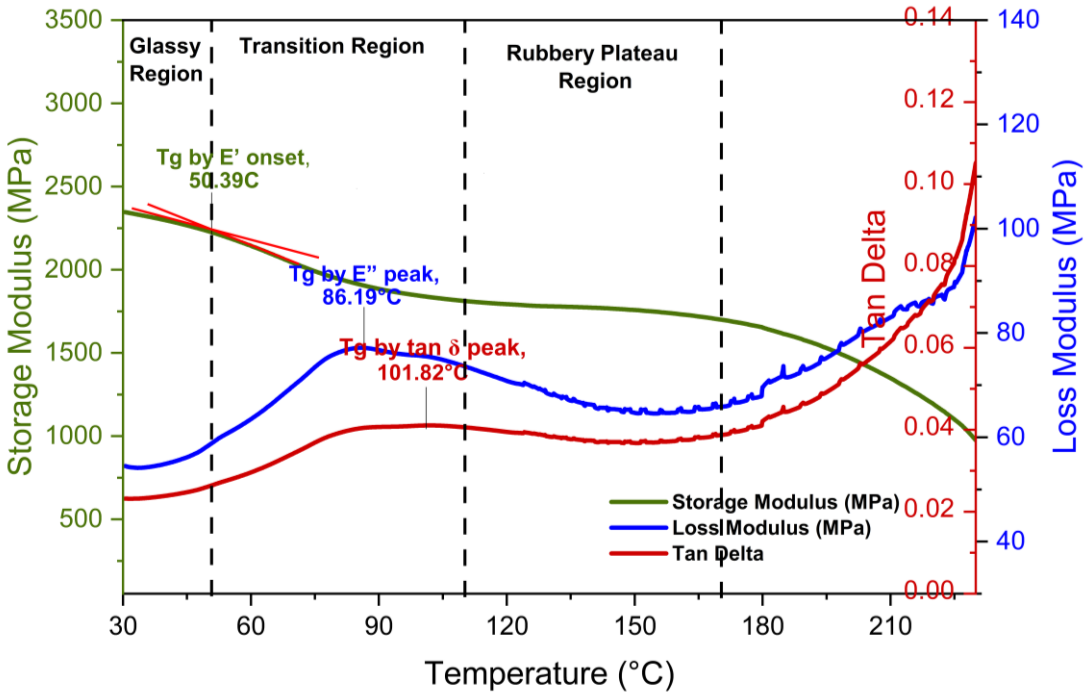

Fig. 4. DMA graphs for Batai (*Paraserianthes falcataria*) with storage modulus (*E'*), loss modulus (*E"*), and damping factor (tan *δ*) with temperature at 1 Hz, showing the three principal phases; glassy region, transition region, and rubbery plateau regions

The stages are: glassy (0 to 50 °C); viscoelastic (50 to 110 °C); and rubbery (110 to 250 °C). Each stage exhibits distinct mechanical behaviour, with the glassy phase

associated with high stiffness, the rubbery phase with greater flexibility, and the transition phase capturing the progressive shift between the two. These changes are manifested in the evolution of the storage modulus (E'), loss modulus (E''), and loss factor (tan δ) as a function of temperature. Under fire or elevated thermal exposure, the progression from glassy to rubbery behaviour is critical, as it governs stiffness retention, damping capacity, and ultimately the onset of mechanical degradation that accelerates charring and structural failure.

Figure 4 also shows three distinct relaxation events identified at approximately 50 °C (E' onset temperature), 86 °C (E'' peak temperature), and 101 °C (tan δ peak temperature). As temperature increases, the wood polymers progressively gain molecular mobility, leading to a reduction in the storage modulus (E') and the appearance of distinct peaks in the loss factor (tan δ). These changes signal the transition from the glassy to the rubbery state and are associated with specific molecular relaxations. The second relaxation, typically observed in the range of 60 to 100 °C, is attributed to the softening of hemicelluloses, which are highly hygroscopic and particularly sensitive to moisture-assisted mobility (Salmén 1984; Olsson and Salmén 2004). The peaks of E'' and tan δ are positioned in the transition region. At higher temperatures, a third relaxation occurs, reflecting the onset of lignin softening and the gradual activation of its aromatic network (Kelley *et al.* 1987). These sequential relaxation events illustrate the differing thermal responses of wood's amorphous components, with hemicellulose governing early-stage viscoelastic transitions and lignin controlling high-temperature softening, both of which strongly influence stiffness retention and damping under elevated temperatures (Bartlett *et al.* 2019).

The effects of frequency (1, 2, and 5 Hz) on dynamic properties of both species were determined to quantify the shift in glass transition temperature (T_g). The storage modulus, tan delta and loss modulus *versus* temperature plots for 3 frequencies for Batai and Laran are presented in Figs. 5 and 6, respectively.

The DMA trends for Batai and Laran were consistent with viscoelastic theory for wood, showing clear frequency- and species-dependent differences in storage modulus (E'), loss modulus (E''), and damping behaviour (tan δ). Across the frequency range of 1 to 5 Hz, both species exhibited decreasing E' with increasing temperature, reflecting the progressive softening of amorphous cell-wall constituents. Laran maintained consistently higher E' values than Batai at most temperatures, indicating a stiffer matrix and stronger rate sensitivity, whereas Batai displayed lower stiffness but greater sensitivity to frequency. This can be related to density of Laran (600 kg/m^3) is higher than density of Batai (400 kg/m^3). However, at 1 Hz where Batai showed a slightly higher E' at the onset of the storage modulus curve. This indicates that Batai retains greater stiffness under low-frequency loading, while Laran demonstrates superior rate sensitivity, responding more effectively to higher loading frequencies.

In contrast to E', the damping response (tan δ) was markedly more sensitive to frequency because tan δ is defined as the ratio of the viscous to elastic components (tan $\delta = E''/E'$) (Menard and Menard 2015). Therefore, relatively small frequency-driven changes in E'' (energy dissipation) can produce larger apparent changes in tan δ, whereas E' (energy storage) is typically dominated by the load-bearing cell-wall framework and therefore varies more modestly over a narrow frequency window (Salmén 1984; Kelley *et al.* 1987).

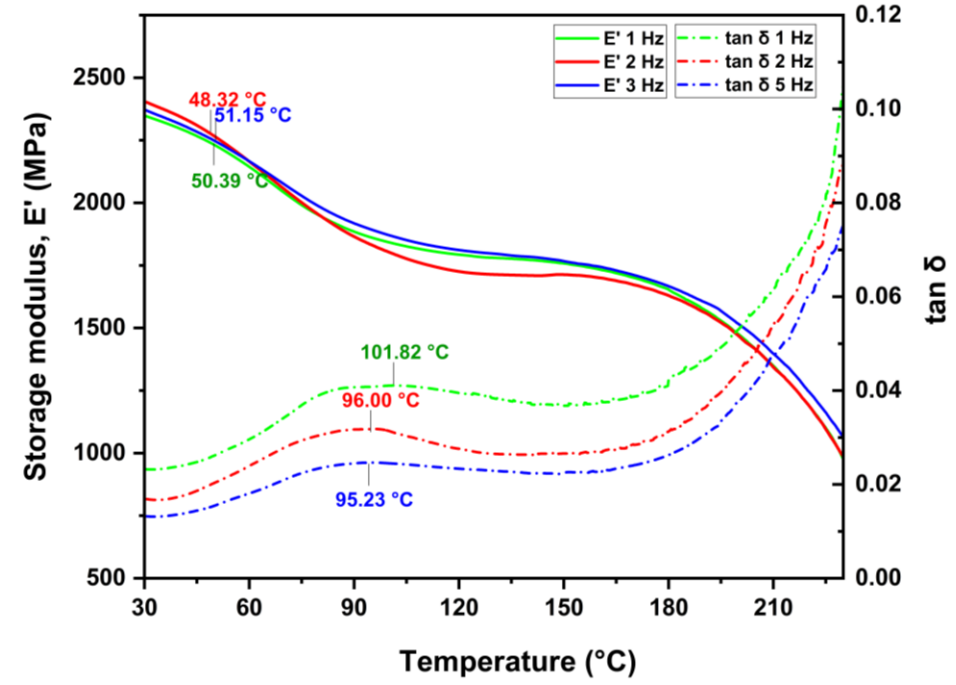

(a)

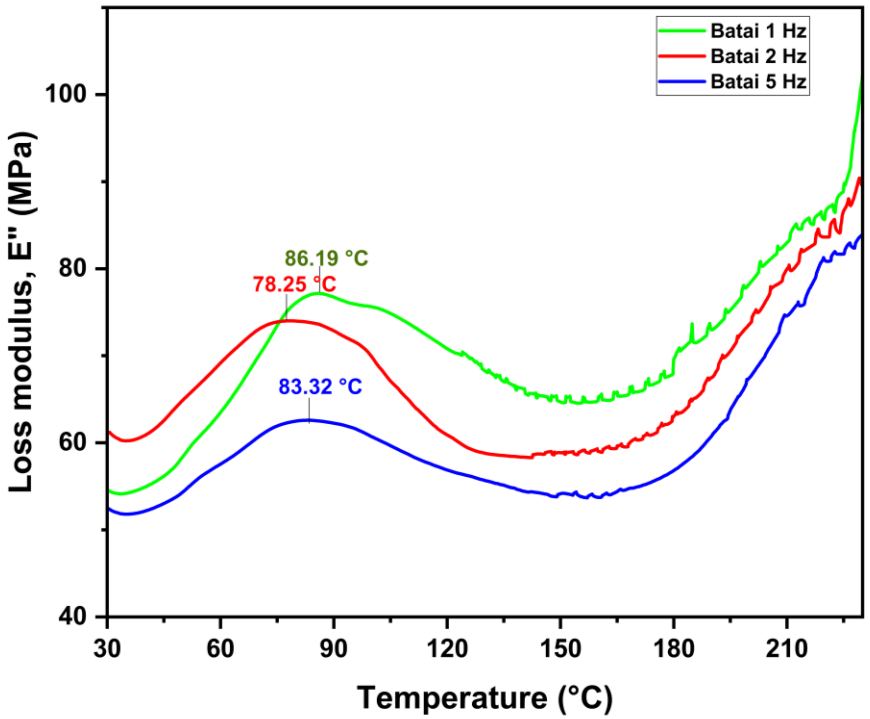

(b)

Fig. 5. DMA graphs for Batai (*Paraserianthes falcataria*) at 1 Hz, 2 Hz, and 5 Hz showing: (a) storage modulus (*E'*) and tan δ and (b) loss modulus (*E''*)

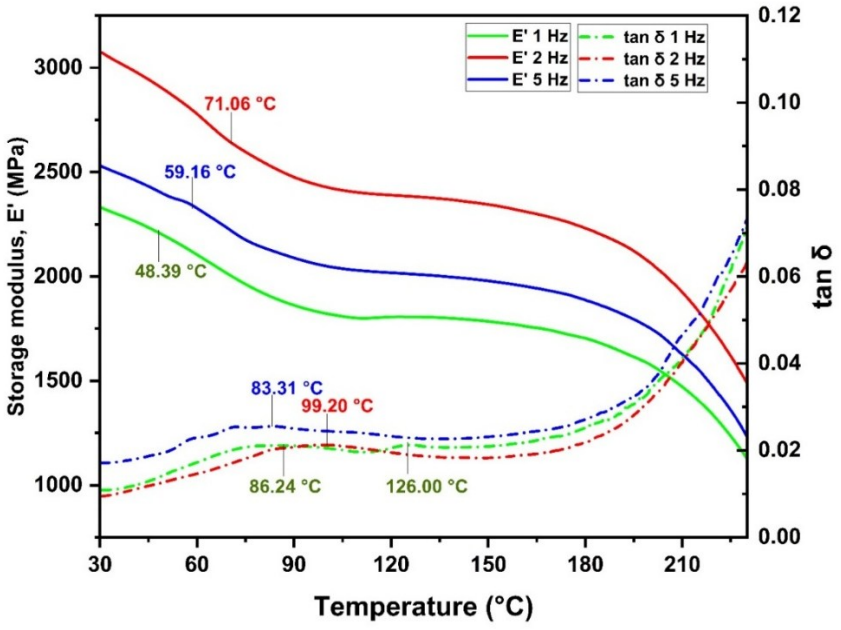

(a)

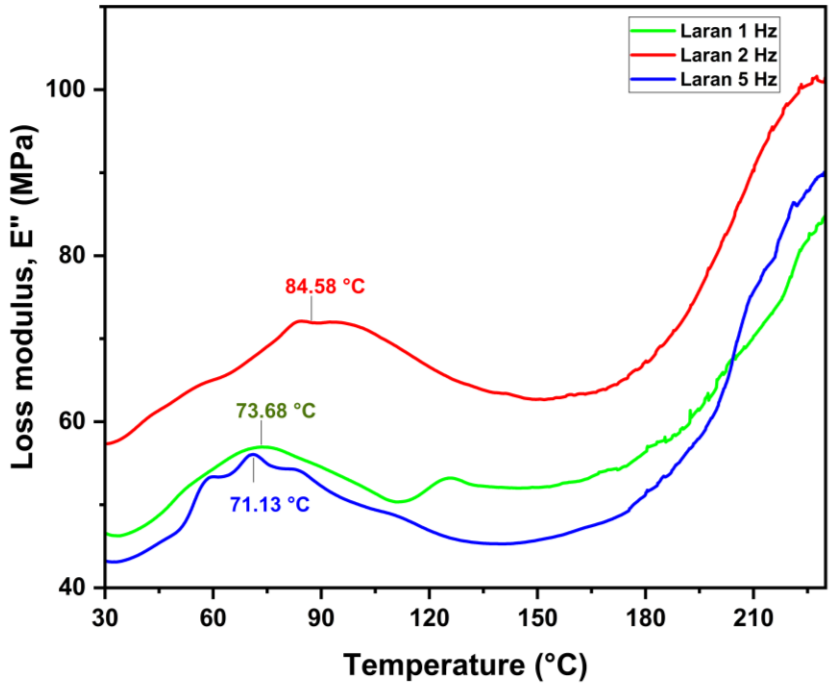

(b)

Fig. 6. DMA graph of Laran (*Neolamarckia cadamba*) at 1 Hz, 2 Hz, and 5 Hz showing: (a) storage modulus (*E'*) and tan δ and (b) loss modulus (*E"*)

In wood, *E"* and tan δ are governed by rate-dependent molecular motions in amorphous constituents (particularly hemicellulose- and lignin-associated relaxations, and moisture-assisted mobility) (Salmén 1984; Sun *et al.* 2007), so increasing frequency restricts segmental motion and shifts/broadens the damping transition (Menard and Menard

2015; Ashaduzzaman *et al.* 2020). Accordingly, the pronounced frequency dependence observed in tan δ is consistent with time-dependent relaxation processes, while the comparatively smaller frequency effect on E' reflects the more elastic, structure-dominated contribution to stiffness under the present test condition (Kelley *et al.* 1987; Kutnar *et al.* 2021).

Similar temperature and frequency dependent reductions in E' have been reported for Scots pine and several tropical hardwoods (*e.g.*, Gmelina, Obeche, Alstonia), which can be attributed to thermally activated molecular motions captured by the time–temperature superposition principle (Salmén 1984; Ashadduzaman *et al.* 2020). These species-specific differences are consistent with Laran's denser anatomy and potentially more aligned microfibril structure, which promote stiffness (Hamdan *et al.* 2010), while Batai's lower modulus reflects its lightweight, plantation grown nature, characterized by lower density and higher porosity.

For Batai, E' values at room temperature ranged between 2300 and 2500 MPa, increasing systematically with frequency from 1 to 5 Hz. This behavior is typical of viscoelastic materials, where faster oscillatory loading restricts molecular mobility, thereby enhancing apparent stiffness. As temperature increased, E' declined steadily, with sharper reductions beyond 180 °C, although the frequency effect was maintained, with the 5 Hz curve consistently above those at 1 and 2 Hz. In contrast, Laran displayed higher initial stiffness, ranging from 2300 to over 3100 MPa, with E' exceeding 3000 MPa at 2 Hz. However, the differences between frequencies were more pronounced than in Batai, and although Laran retained higher absolute stiffness across the full temperature range, it also showed a steeper modulus decline above 150 °C. Taken together, these results suggest that Batai exhibits more pronounced frequency dependence and better stiffness retention at elevated temperatures, whereas Laran, despite its greater inherent stiffness, demonstrates a more elastic-dominated response with reduced damping.

The tan δ profiles in Fig. 7(a) highlight the contrasting damping behaviours of the two species. Batai consistently exhibited higher tan δ values across all frequencies, indicating greater damping capacity and energy dissipation. At 1 Hz, sharper and more pronounced tan δ peaks compared to Laran were observed around 70 to 100 °C, corresponding to hemicellulose relaxations and moisture-assisted mobility within the amorphous cell wall matrix (Jakes 2019). At higher frequencies (2 to 3 Hz), these peaks broadened and shifted slightly to lower temperatures, while their intensity diminished, indicating a transition towards more elastic-dominated behaviour. In contrast, Laran displayed generally lower tan δ values across frequencies, signifying reduced internal friction and a stiffer, more elastic character. Its peaks were broader and less intense, even during the glassy-to-rubbery transition, reflecting limited damping. This behaviour is consistent with Laran's higher lignin and hemicellulose content, which provide stiffness and structural rigidity but restrict molecular mobility and energy dissipation (Kelley *et al.* 1987; Backman and Lindberg 2001).

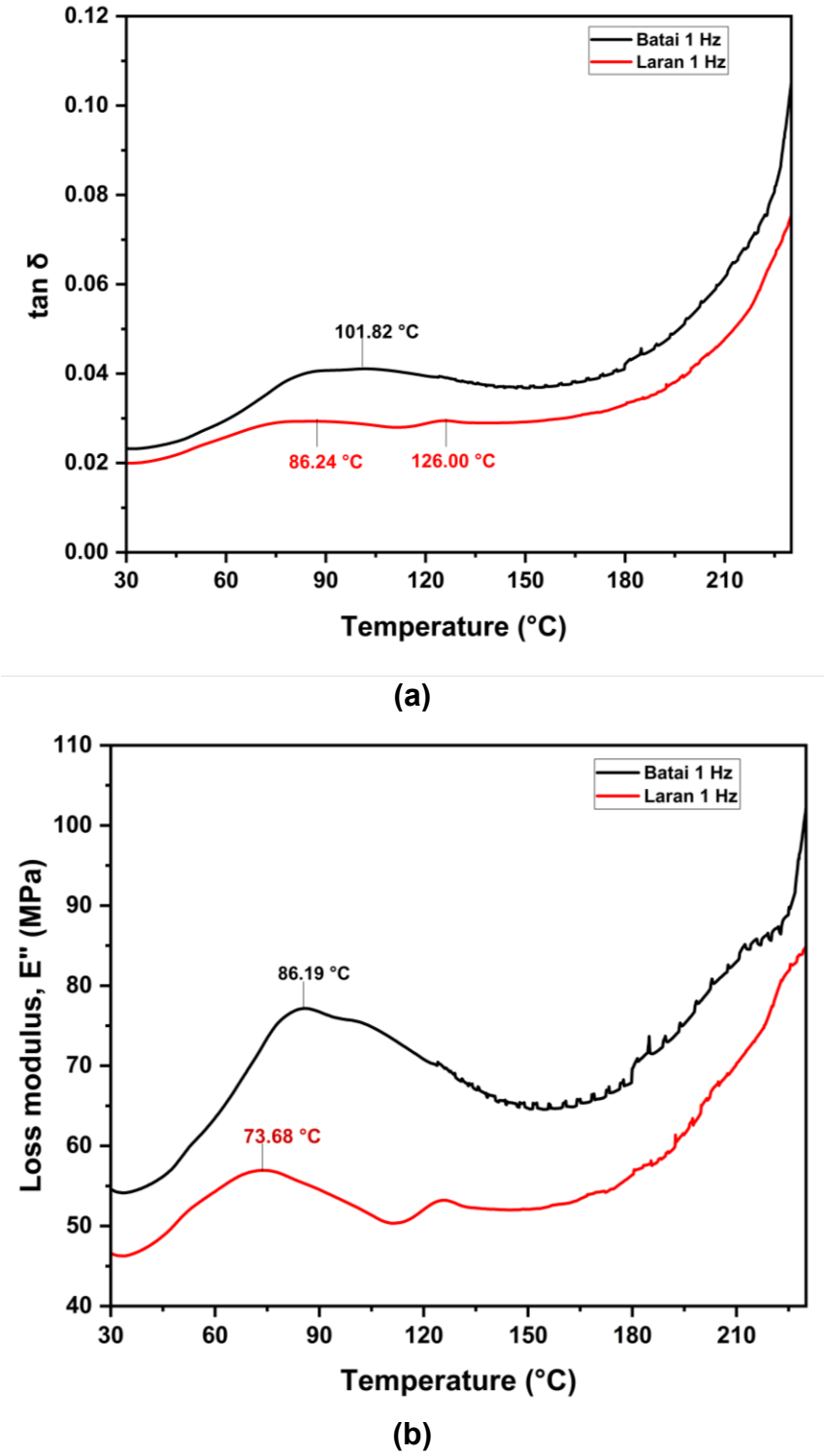

Fig. 7. Comparison between Batai (*Paraserianthes falcataria*) and Laran (*Neolamarckia cadamba*) at 1 Hz: (a) tan δ and (b) loss modulus

The loss modulus (E'') further illustrates these differences. For Batai, distinct relaxation peaks were evident: ~86 °C at 1 Hz, ~78 °C at 2 Hz, and ~83 °C at 3 Hz, consistent with hemicellulose relaxations. At higher temperatures (> 150 °C), all curves exhibited secondary increases in E'', corresponding to lignin softening. Importantly, the

magnitude of E'' decreased as frequency increased, confirming reduced damping capacity at higher oscillation rates. Laran, however, showed weaker relaxation peaks between 71 °C and 85 °C, with less frequency sensitivity. The magnitude of its peaks was smaller than Batai's, as can be seen in Fig. 6(b), indicating lower damping efficiency. At elevated temperatures, E'' rose gradually across all frequencies, but the curves remained closely spaced, again pointing to Laran's weaker frequency dependence.

Between species, the contrasts were clear where Batai demonstrated greater damping, reflected in higher tan δ values and sharper E'' peaks, while Laran consistently provided higher stiffness but at the expense of energy dissipation. These differences align with species-specific polymer composition and lignin–hemicellulose interactions (Bartlett *et al.* 2019). From a performance standpoint, Batai's stronger damping makes it more suitable for applications requiring vibration control and thermal energy dissipation, while Laran's superior stiffness but limited damping favours load-bearing applications where stiffness retention is paramount, particularly under fire or mechanical loading.

Glass transition temperature (T_g)

Wood, as a natural composite of cellulose, hemicellulose, and lignin, exhibits pronounced viscoelastic behaviour, where its mechanical response depends not only on the applied stress or strain but also on time, temperature, and moisture conditions. Among the key performance indicators derived from DMA, the glass transition temperature (T_g) is particularly important. The T_g marks the transition of the amorphous regions of wood polymers from a rigid, glassy state to a more flexible, rubbery state, where chain segments gain mobility and energy dissipation increases. Identifying T_g provides a benchmark for predicting how wood will perform under fluctuating thermal environments, such as those encountered in service or during fire exposure. A higher or more stable T_g is generally associated with improved stiffness retention at elevated temperatures, whereas a lower T_g may indicate earlier onset of softening and reduced load-bearing capacity. Thus, T_g is not only a fundamental material parameter but also a practical predictor of wood's dimensional stability, creep resistance, and fire performance. From DMA study, the T_g can be determined from onset temperature value of storage modulus curve, peak temperature of loss modulus curve, or peak temperature of tan δ curve.

The glass transition region was evaluated using the onset of storage modulus (E') reduction, the peak of the loss modulus (E''), and the peak of tan δ. Table 1 shows the glass transition temperatures at different frequencies. In general, the T_g from these three methods yielded values in the order: T_g, onset (E') < T_g, E'', < T_g, tan δ. Although the storage modulus (E') generally showed a marked decline as the temperature approached T_g, this change was more gradual and can be difficult to pinpoint precisely. In contrast, the tan δ peak offers a sharper and more distinctive signal, making it the most reliable indicator of T_g. Previous studies on different wood species consistently demonstrate this behavior, highlighting that the tan δ criterion allows for more accurate and reproducible T_g determination than relying solely on the storage modulus drop (Obataya *et al.* 2000; Ashaduzzaman *et al.* 2020; Kutnar *et al.* 2021).

For Batai, the E' onset occurred between approximately 48 to 51°C, with E'' peaks between 78 to 86 °C and tan δ peaks ranging from 95 to 102 °C across the tested frequencies. For Laran, the E' onset was observed between 48 to 71 °C, E'' peaks between 71 to 85 °C, and tan δ peaks from 83 to 126 °C.

Table 1. Glass Transition Temperature at *E'*, *E''*, and tan δ Curve with Corresponding *E'* Values

Sample	Frequency (Hz)	T_g(°C) (Onset *E'* Curve)	*E'* at Onset *E'* Curve Temp. (MPa)	T_g(°C) (Peak *E''* Curve)	*E'* at Peak *E''* Curve (MPa)	T_g(°C) (Peak tan δ Curve)	*E'* (MPa) at Peak tan δ Curve Temp.
Batai (*Paraserianthes falcataria*)	1	50.4	2228	86.2	1906	101.8	1838
	2	48.3	2280	78.3	1967	96.0	1825
	5	51.2	2240	83.3	1961	95.2	1893
Laran (*Neolamarckia cadamba)*	1	48.4	2208	73.7	1973	126.0	1806
	2	71.1	2650	84.6	2514	99.2	2431
	5	59.2	2340	71.1	2213	83.3	2123

In dynamic mechanical analysis (DMA), the glass transition temperature (T_g) is inherently frequency dependent, with higher test frequencies generally yielding higher apparent T_g values due to the kinetically controlled nature of viscoelastic relaxation. At shorter observation times, greater thermal energy is required for polymer chain segments to respond, shifting the transition to higher temperatures. The observed inconsistencies in T_g trends between the two timbers across frequencies therefore reflect material-related effects. Wood is a heterogeneous, multi-phase polymeric composite, and the T_g detected by DMA, primarily associated with lignin softening and is influenced by interactions with hemicellulose, moisture, and extractives, leading to broadened or overlapping relaxations and non-uniform frequency shifts. In addition, differences in moisture content (bound water) and hygroscopicity alter molecular mobility through plasticisation effects, further affecting T_g –frequency sensitivity. Microstructural constraints such as density, cell wall thickness, and polymer network rigidity also influence relaxation behaviour, resulting in species-dependent T_g responses even under identical DMA conditions.

Batai exhibited sharper tan δ peaks with higher magnitudes, while Laran showed broader and less intense peaks. These results highlight contrasting relaxation behaviours between the two species. The sharper, more pronounced tan δ peaks of Batai indicate a more homogeneous amorphous phase and greater damping capacity, consistent with its lower lignin content and more ordered cellulose domains observed in FTIR (Backman and Lindberg 2001; Colom *et al.* 2003; Bartlett *et al.* 2019). In contrast, Laran displayed broader and less intense transitions, reflecting multiple overlapping relaxations due to its higher lignin and hemicellulose content (Faix 1991; Poletto *et al.* 2014; Wang *et al.* 2017). This compositional profile corresponds to its higher stiffness (*E'*) and reduced energy dissipation, confirming that Batai is more effective in damping applications, while Laran offers superior stiffness across a wider temperature range.

FTIR Analysis

The FTIR spectroscopy was employed to characterize the chemical composition and functional groups of Batai and Laran wood particles. FTIR provides a molecular fingerprint of lignocellulosic materials by probing the vibrational modes of cellulose, hemicellulose, and lignin, which collectively determine the structural and thermal performance of wood. The spectra were recorded in transmittance (%T) mode, where lower %T values (deeper troughs) correspond to stronger absorbance and thus higher relative abundance of the associated chemical groups. Typical wavenumber assignments for lignocellulosic polymers are summarized in Table 2 and include hydroxyl stretching (3600

to 3200 cm^{-1}), C–H stretching (2950 to 2850 cm^{-1}), carbonyl stretching (1720 to 1740 cm^{-1}), aromatic skeletal vibrations (1610 to 150 cm^{-1}), and carbohydrate-related C–O stretching (1200 to 900 cm^{-1}) (Pandey 1999; Colom *et al.* 2003; Poletto *et al.* 2012).

Table 2. FTIR Wavenumber Regions and Corresponding Functional Groups in Wood Based on Literature*

Wavenumber Range (cm^{-1})	Functional Group / Vibration	Assignment in Wood/Biomass
3600 to 3200	O–H stretching	Hydroxyl groups in cellulose, hemicellulose, lignin, and absorbed water
2950 to 2850	C–H stretching (–CH_2, –CH_3)	Aliphatic C–H in cellulose, hemicellulose, and lignin side chains
1720 to 1740	C=O stretching (ester, carbonyl)	Acetyl/uronic ester in hemicellulose; carbonyl in extractives
1660 to 1630	O–H bending / C=C stretching	Absorbed water; aromatic skeletal vibration in lignin
1610 to 1500	Aromatic C=C stretching	Aromatic skeletal vibration in lignin (guaiacyl, syringyl units)
1470 to 1450	C–H deformation (–CH_2/–CH_3)	Deformation vibration in cellulose and lignin
1375 to 1320	O–H bending, C–H wagging	Cellulose and hemicellulose
1270 to 1210	C–O stretching (aryl–O)	Syringyl ring vibration + C–O stretching in lignin/hemicellulose
1165 to 1110	C–O–C asymmetric stretching	β-glycosidic linkages in cellulose and hemicellulose
1060 to 1000	C–O stretching (alcohols, ethers)	C–O stretching in cellulose/hemicellulose (fingerprint region)
900 to 890	C–H deformation (out-of-plane)	β-glycosidic linkage in cellulose; indicator of polysaccharides

*Apayidin *et al.* 2023; Colom *et al.* 2003; Fellak *et al.* 2022; Gaitán-Álvarez *et al.* 2020; Horiyama *et al.* 2023; Oh *et al.* 2005; Pandey 1999; Poletto *et al.* 2012; Traoré *et al.* 2018)

Comparative spectra of Batai and Laran

Figure 8 presents the FTIR transmittance spectra of Batai and Laran wood samples in the range of 4000 to 500 cm^{-1}, highlighting the characteristic functional groups associated with the major wood constituents—cellulose, hemicellulose, and lignin. The main peak assignments and their relative transmittance values are summarized in Table 3. While both spectra display the typical absorption bands of lignocellulosic materials, noticeable differences in peak intensity and transmittance levels reflect variations in chemical composition and molecular bonding between the two species.

Although spectra were acquired in transmittance (%T) mode, where lower %T values correspond to stronger absorption, absolute band intensities may be influenced by global spectral scaling effects, including variations in sample loading, optical path length, and light scattering. Consequently, spectral interpretation was based primarily on relative band behaviour, such as changes in band shape and relative intensity. Where appropriate, band intensities were normalised to a comparatively stable carbohydrate-related band within the fingerprint region to minimise inter-spectrum intensity bias.

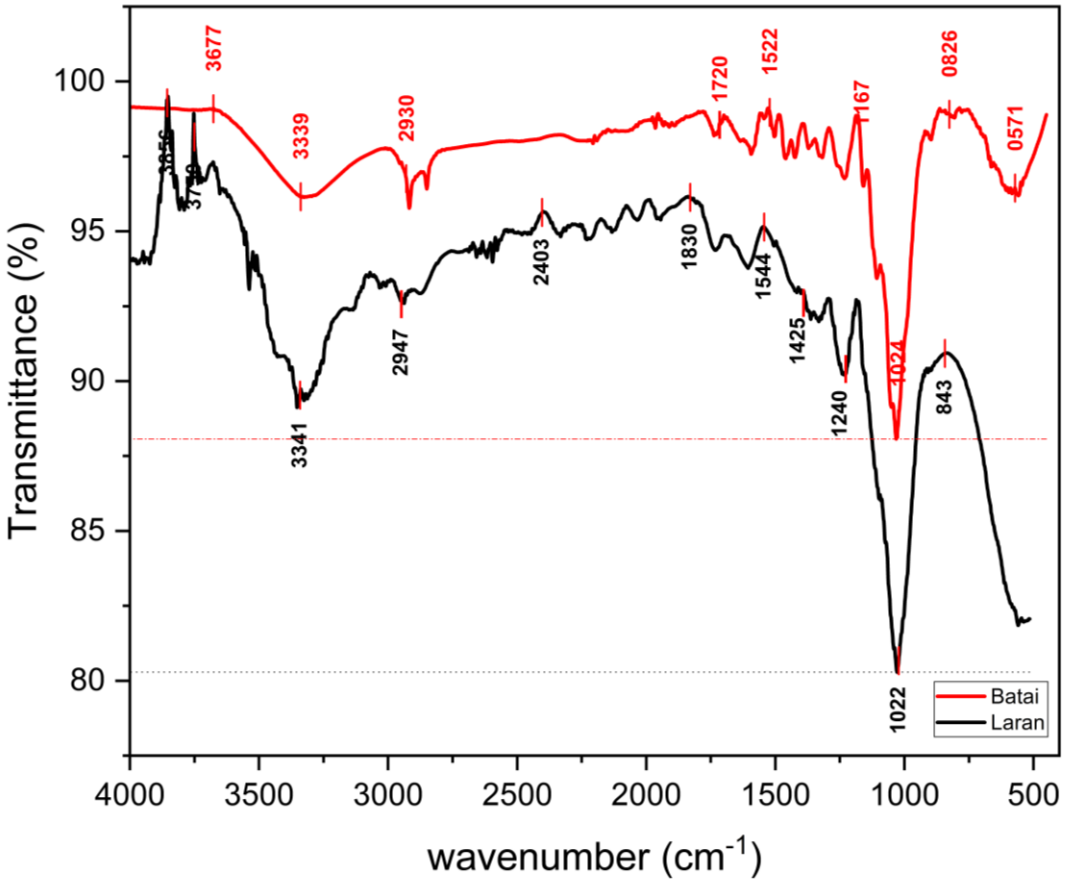

Fig. 8. FTIR spectra of Batai (*Paraserianthes falcataria*) and Laran (*Neolamarckia cadamba*) showing distinct chemical composition differences

Table 3. FTIR Band Assignments and Observed Differences Between Batai and Laran

Wavenumber Range (cm^{-1})	Functional Group / Assignment	Wavenumber Observed (cm^{-1})	%T	
			Batai	Laran
3600 to 3200	O–H stretching (cellulose, hemicellulose, lignin)	~3340	96	89
2950 to 2850	C–H stretching (–CH_2, –CH_3 in polysaccharides, lignin)	~2930	96	92
1740 to 1720	C=O stretching (hemicellulose acetyl, lignin carbonyl)	~1720	98	94
1600 to 1510	Aromatic skeletal vibrations (lignin)	~1520	98	94
1460 to 1420	C–H bending (cellulose, lignin)	~1425	98	93
1260 to 1230	C–O stretching (lignin, guaiacyl units)	~1240	96	90
1200 to 900	C–O–C, C–O stretching (cellulose, hemicellulose)	~1025	88	80
840 to 820	Aromatic C–H out-of-plane bending (lignin)	~840	98	90
Approx. 570 to 600	Skeletal vibrations (cellulose)	~571	96	82

The hydroxyl stretching (3600 to 3200 cm^{-1}) and O–H centered at ~3340 cm^{-1} were present in both species, but with different features. The broad absorption band observed around 3341 to 3339 cm^{-1} corresponds to the O–H stretching vibration of hydroxyl groups in cellulose, hemicellulose, and absorbed moisture.

Laran exhibited a stronger and broader absorbance (lower %T, ~89%T) compared to Batai (~96%T). This stronger absorbance is attributed to the presence of amorphous hemicellulose and lignin hydroxyl groups, which contribute to hydrogen bonding networks with less structural order (Poletto *et al.* 2014), which is often associated with higher hygroscopicity and moisture affinity. This is also suggesting a higher contribution from bound moisture and/or more accessible hydroxyl functionalities compared with Batai. This interpretation is supported by the presence of a weak feature near ~1630 to 1650 cm^{-1} (H–O–H bending of absorbed water), which is slightly more evident in Laran. This observation is consistent with reported relationships between wood density, microstructure, and hydroxyl group availability (Ansell 1985).

In contrast, Batai displayed a sharper O–H band, which is typically associated with crystalline cellulose domains, where intramolecular hydrogen bonds are more ordered and compact (Colom *et al.* 2003). This suggests that Batai contains more ordered cellulose regions compared to Laran. Although the O–H region may also include contributions from absorbed moisture, the samples were stored under dry conditions prior to analysis; therefore, compositional differences are considered the primary driver of the observed contrast.

The peaks at approximately 2950 to 2850 cm^{-1} are attributed to C–H stretching of aliphatic $–CH_2$ and $–CH_3$ groups, primarily from cellulose and hemicellulose. Weak absorbance in this region is linked to aliphatic C–H stretching vibrations of $–CH_2$ and $–CH_3$ groups in polysaccharides and lignin side chains. Laran exhibited slightly stronger intensity, suggesting a marginally higher contribution of carbohydrate structures or a denser molecular packing, reflecting the contribution of lignin side groups and hemicellulose branching. Although subtle, this difference supports the observation that Laran is chemically more heterogeneous, whereas the higher transmittance of Batai is consistent with its lower density and more porous structure.

The carbonyl stretching region (~1740 to 1720 cm^{-1}), with an absorbance at ~1720 cm^{-1}, was more pronounced in Laran (~94%T) than in Batai (~98%T). This band is commonly assigned to unconjugated C=O stretching associated with acetyl groups in hemicellulose and ester linkages in lignin (Lionetto *et al.* 2012; Kubovský *et al.* 2020).

Laran also showed a stronger aromatic skeletal vibration (1600 to 1500 cm^{-1}) at ~1520 cm^{-1}, corresponding to aromatic skeletal vibrations of guaiacyl and syringyl units in lignin (Faix 1991). This indicates that Laran has a higher lignin fraction compared to Batai which is consistent with the generally higher density and superior fire resistance. The higher lignin contribution in Laran is consistent with its greater stiffness observed in DMA, because lignin contributes to rigidity in the cell wall (Fellak *et al.* 2022). Lignin is known to play a dominant role in char formation and thermal stability, making this difference particularly relevant for fire-performance interpretation.

The complex region between 1450 and 1200 cm^{-1} is associated with C–H deformation and C–O stretching in cellulose, hemicellulose, and lignin. Peaks observed at 1425 cm^{-1} (CH_2 scissoring in cellulose) and 1240 cm^{-1} (C–O stretching in lignin and hemicellulose) are present in both species. For Batai, the C–H band at ~1425 cm^{-1} was sharper and more distinct in shape, which is often associated with more ordered cellulose regions (Oh *et al.* 2005). However, the transmittance values indicate that Laran had

stronger absorbance at ~1425 cm^{-1} (93%T) and ~1030 cm^{-1} (80%T at 1022 cm^{-1}) compared to Batai (98%T and 88%T, respectively). The absorption band at approximately 1022 to 1024 cm^{-1} was assigned to C–O–C and C–O stretching vibrations of polysaccharides, particularly cellulose. This suggests that while Batai may have slightly more ordered cellulose domains (narrower peaks), Laran exhibits higher overall cellulose/hemicellulose absorbance intensity reflecting a higher structural integrity of carbohydrate network. The less compact carbohydrate framework in Batai may contribute to its faster thermal degradation and lead to lower stiffness in DMA. The band at ~840 cm^{-1}, corresponding to aromatic C–H out-of-plane deformation in lignin, was stronger in Laran, reinforcing its higher lignin content. The clearer presence of this peak in Laran further supports the conclusion of a more ordered cellulose structure compared to Batai. Similarly, at ~571 cm^{-1}, Laran (82%T) again showed stronger absorbance than Batai (96%T). Although Batai's peaks appear sharper, the stronger absorbance in Laran indicates a more chemically heterogeneous structure enriched in lignin and hemicellulose (Pandey 1999; Traoré *et al.* 2018).

Overall, Table 3 and Fig. 8 demonstrate that while both species share the fundamental chemical features of lignocellulosic biomass, their relative chemical signatures are distinct. In general, Batai shows higher transmittance across most regions, reflecting lower chemical density and weaker intermolecular interactions. The FTIR results show that Batai is dominated by crystalline cellulose, with sharper and more defined carbohydrate and skeletal vibrations, while Laran possesses higher hemicellulose and stronger lignin-related aromatic structures and more pronounced carbohydrate bonding, as evidenced by its stronger O–H, C=O, aromatic, and 840 cm^{-1} bands. These findings demonstrate that Batai has a more ordered and crystalline structure, whereas Laran possesses a more chemically heterogeneous and amorphous matrix. These FTIR findings align well with the DMA results, where Batai showed higher damping capacity associated with its more mobile amorphous domains, and Laran displayed higher stiffness due to its lignin-rich matrix.

Correlation with viscoelastic behaviour

The FTIR spectra and DMA results exhibit a clear and internally consistent relationship between the chemical composition and thermo-mechanical behaviour of the two wood species. In the FTIR analysis, Batai showed more pronounced carbohydrate-associated bands at approximately 1425 and 1030 cm^{-1}, which is commonly attributed to CH_2 scissoring and C–O–C stretching in cellulose. These features suggest relatively well-defined cellulose domains (Poletto *et al.* 2012a; Oh *et al.* 2005), but they were accompanied by weaker aromatic lignin (~1510 to 1525 cm^{-1}) and carbonyl (~1720 cm^{-1}) bands, indicating a lower lignin contribution and fewer chemically constrained domains. This compositional profile corresponds closely with the DMA response of Batai, which exhibited lower E' values (reduction in stiffness), higher tan δ values and higher loss modulus (E''), reflecting greater energy dissipation and molecular mobility. Importantly, the increased damping observed in Batai is not attributed to cellulose crystallinity itself, but rather to the reduced lignin content and more accessible amorphous regions, which facilitate thermally activated segmental motion and viscous response (Salmén 1984; Backman and Lindberg, 2001; Bartlett *et al.* 2019).

In contrast, Laran displayed stronger absorption in the carbonyl (~1720 cm^{-1}) and aromatic lignin (~1510 to 1525 cm^{-1}) regions, consistent with a higher lignin and hemicellulose content and a more crosslinked polymeric network (Faix 1991). This

chemical signature is reflected in its DMA behaviour, where lower tan δ values and lower E'' values, and a broader relaxation transition were observed, together with higher stiffness (E'). The lignin-rich matrix in Laran effectively restricts chain mobility, resulting in reduced damping capacity and delayed relaxation, while simultaneously promoting greater modulus retention up to elevated temperatures. However, once softening initiates, the constrained network leads to a more pronounced modulus loss as thermal activation overcomes molecular restrictions (Kelley *et al.* 1987; Fellak *et al.* 2022).

At elevated temperatures above ~150 °C, both species showed a rapid increase in tan δ accompanied by a sharp decline in E', indicating the onset of pronounced thermal softening. However, the lower E'' and tan δ values of Laran prior to this transition suggest superior resistance to thermally induced molecular motion, whereas Batai undergoes earlier and more intense viscous relaxation. This behaviour is consistent with the role of lignin as a thermally stable, load-bearing component that enhances stiffness but limits damping.

It should be noted that while FTIR provides valuable insight into chemical functionality and relative compositional differences, it does not capture anatomical and ultrastructural parameters—such as microfibril angle, cell-wall layering, density, and microstructural heterogeneity—which are also known to influence viscoelastic behaviour. Consequently, although the strong agreement between FTIR and DMA supports a composition-driven interpretation, the observed differences in E' and tan δ may also partially reflect microstructural contributions not quantified in the present study. Overall, the combined FTIR–DMA analysis confirms that Batai, characterised by lower lignin content and more mobile amorphous domains, exhibits greater damping capacity, whereas Laran, dominated by lignin- and hemicellulose-rich structures, demonstrates higher stiffness but reduced energy dissipation under thermal loading.

These viscoelastic differences have direct implications for thermal and fire behaviour. The lower damping and reduced molecular mobility of Laran suggest enhanced resistance to thermal softening and improved char stability, consistent with its stronger lignin signature. Conversely, the higher damping and earlier relaxation of Batai imply a greater tendency for softening and volatile release at elevated temperatures, which may contribute to earlier ignition and faster thermal degradation under fire exposure.

CONCLUSIONS

1. The integration of dynamic mechanical analysis (DMA) with Fourier-transform infrared (FTIR) spectroscopy proved effective in analyzing the thermo-mechanical and chemical responses of tropical plantation woods, providing a comprehensive understanding of their properties.
2. Batai exhibited superior damping and sharper glass transition peaks, which are attributed to its lower lignin content and more ordered cellulose domains, suggesting its potential advantage in applications requiring vibration damping and energy dissipation.
3. Laran demonstrated higher stiffness and broader, less distinct glass transition peaks due to its lignin- and hemicellulose-enriched matrix, making it more suitable for load-bearing applications where stiffness is crucial.

4. The DMA–FTIR approach allowed a direct correlation between modulus loss, damping, and molecular-level degradation, offering a mechanistic understanding of stiffness retention and energy dissipation under elevated temperatures.

ACKNOWLEDGMENTS

The authors gratefully acknowledge the Sarawak Timber Industry Development Corporation (STIDC) for its support and funding of this research under the Strategic Research Partnership (Grant No. 100-RMC 5/3/SRP PRI (043/2024). Special thanks are extended Research Management Centre at Universiti Teknologi MARA (UiTM), Faculty of Civil Engineering and Faculty of Chemical Engineering, UiTM for their invaluable laboratory and administrative support.

REFERENCES CITED

Ansell, M. P. (1985). "Wood microstructure – A cellular composite," in: M. P. Ansell (ed.), *Wood Composites*, Butterworth-Heinemann, pp. 3-26. https://doi.org/10.1016/B978-1-78242-454-3.00001-9

Apaydın Varol, E., and Mutlu, Ü. (2023). "TGA-FTIR analysis of biomass samples based on the thermal decomposition behavior of hemicellulose, cellulose, and lignin," *Energies* 16(9), article 3674. https://doi.org/10.3390/en16093674

Ashaduzzaman, M., Hale, M., Ormondroyd, G., and Spear, M. (2020). "Dynamic mechanical analysis of Scots pine and three tropical hardwoods," *International Wood Products Journal* 11(4), 189-203. https://doi.org/10.1080/20426445.2020.1799910

Backman, A. C., and Lindberg, K. A. H. (2001). "Differences in wood material responses for radial and tangential directions as measured by dynamic mechanical thermal analysis," *Journal of Materials Science* 36(15), 3777-3783. https://doi.org/10.1023/A:1017986119559

Bartlett, A. I., Hadden, R. M., and Bisby, L. A. (2019). "A review of factors affecting the burning behaviour of wood for application to tall timber construction," *Fire Technology* 55(1), 1-49.

Colom, X., Carrillo, F., Nogués, F., and Garriga, P. (2003). "Structural analysis of photodegraded wood by means of FTIR spectroscopy," *Polymer Degradation and Stability* 80(3), 543-549. https://doi.org/10.1016/S0141-3910(03)00051-X

Faix, O. (1991). "Classification of lignins from different botanical origins by FT-IR spectroscopy," *Holzforschung* 45(S1), 21-28. https://doi.org/10.1515/hfsg.1991.45.s1.21

Fellak, S., Rafik, M., Haidara, H., Boukir, A., and Lhassani, A. (2022). "Study of natural degradation effect on lignocellulose fibers of archaeological cedar wood: Monitoring by Fourier Transform Infrared (FTIR) spectroscopy," *MATEC Web of Conferences* 360, article 00006. https://doi.org/10.1051/matecconf/202236000006

Ferry, J. D. (1980). *Viscoelastic Properties of Polymers* (3rd Ed.), John Wiley & Sons, Hoboken, NJ, USA.

Gaitán-Álvarez, J., Berrocal, A., Mantanis, G. I., Moya, R., and Araya, F. (2020). "Acetylation of tropical hardwood species from forest plantations in Costa Rica: An

FTIR spectroscopic analysis," *Journal of Wood Science* 66(1), article 49. https://doi.org/10.1186/s10086-020-01898-9

Hamdan, S., Talib, Z. A., Rahman, M. R., Ahmed, A. S., and Islam, M. S. (2010). "Dynamic Young's modulus measurement of treated and post-treated tropical wood polymer composites (WPC)," *BioResources* 5(1), 324-342. https://doi.org/10/15376/biores.5.1.324-342

Havimo, M. (2009). "Dynamic mechanical analysis of wood," *Holzforschung* 63(4), 435-442.

Horiyama, H., Kojiro, K., and Furuta, Y. (2023). "Transition in viscoelastic properties within successive annual rings of radiata pine (*Pinus radiata*)," *Journal of Wood Science* 69(1), article 37. https://doi.org/10.1186/s10086-023-02112-2

Horiyama, H., Miyoshi, Y., Kojiro, K., and Furuta, Y. (2023). "Thermal softening properties of various wood species within an annual ring," *Journal of Wood Science* 69(1), article 30. https://doi.org/10.1186/s10086-023-02104-2

Jakes, J. E., Hunt, C. G., Zelinka, S. L., Ciesielski, P. N., and Plaza, N. Z. (2019). "Effects of moisture on diffusion in unmodified wood cell walls: A phenomenological polymer science approach," *Forests* 10(12), article 1084. https://doi.org/10.3390/f10121084

Junior, M. D. V., Guerrero, F., da Silva, F. M. A., Ramos, G. Q., Matos, R. S., Țălu, Ș., Trong, D. N., and da Fonseca Filho, H. D. (2024). "Thermal decomposition and kinetic analysis of Amazonian woods: A comparative study of *Goupia glabra* and *Manilkara huberi*," *Fire* 7(11), article 390. https://doi.org/10.3390/fire7110390

Kelley, S. S., Rials, T. G., and Glasser, W. G. (1987). "Relaxation behaviour of the amorphous components of wood," *Journal of Materials Science* 22(2), 617-624.

Kubovský, I., Kačíková, D., and Kačík, F. (2020). "Structural changes of oak wood main components caused by thermal modification," *Polymers* 12(2), article 485. https://doi.org/10.3390/polym12020485

Kutnar, A., O'Dell, J., Hunt, C., Frihart, C., Kamke, F., and Schwarzkopf, M. (2021). "Viscoelastic properties of thermo-hydro-mechanically treated beech (*Fagus sylvatica* L.) determined using dynamic mechanical analysis," *European Journal of Wood and Wood Products* 79(2), 263-271. https://doi.org/10.1007/s00107-020-01629-3.

Kutnar, A., Widmann, R., and Brémaud, I. (2013). "Preliminary studies for use of dynamic mechanical analysis (DMA) to verify intensity of thermal wood modifications," *International Wood Products Journal*, 4(3), 158-165. https://doi.org/10.1179/2042645313Y.0000000044

Lee, M. K., and Park, S. H. (2022). "Effects of thermal thickness and charring properties of solid combustibles on heat release and CO emission characteristics," *International Journal of Fire Science and Engineering*, 36(3), 1-8. https://doi.org/10.7731/KIFSE.d131722d

Lionetto, F., Del Sole, R., and Maffezzoli, A. (2012). "Monitoring wood degradation during weathering by cellulose crystallinity," *Materials*, 5(12), 2874-2887.

Liu, I., Wang, S., Zheng, Y., Luo, Z., and Cen, K. (2008). "Mechanism study of wood lignin pyrolysis by using TG–FTIR analysis," *Journal of Analytical and Applied Pyrolysis* 82(1), 170-177. https://doi.org/10.1016/j.jaap.2008.03.007

Meena, M. K., Anand, S., and Ojha, D. K. (2023). "Interdependency of pyrolysis and combustion: A case study for lignocellulosic biomass," *Journal of Thermal Analysis and Calorimetry*, 148, 5509-5519. https://doi.org/10.1007/s10973-023-12090-8

Menard, K. P., and Menard, N. R. (2015). *Dynamic Mechanical Analysis in the analysis of polymers and rubbers* (3rd Ed.), CRC Press, Boca Raton, FL, USA.

Moraes, P. D., Rogaume, Y., Bocquet, J. F., and Triboulot, P. (2005). "Influence of temperature on the embedding strength," *Holz Roh- Werkst.*, 63, 297-302. https://doi.org/10.1007/s00107-004-0568-9

Obataya, E., Higashihara, T., and Tomita, B. (2000). "Hygroscopicity of heat-treated wood. III. Effects on the mechanical properties of wood," *Holzforschung* 54(1), 74-79.

Oh, S. Y., Dong, I. Y., Shin, Y., Hwan, C. K., Hak, Y. K., Yong, S. C., Won, H. P., and Ji, H. Y. (2005). "Crystalline structure analysis of cellulose treated with sodium hydroxide and carbon dioxide by means of X-ray diffraction and FTIR spectroscopy," *Carbohydrate Research* 340(15), 2376-2391. https://doi.org/10.1016/j.carres.2005.08.007

Olsson, A.-M., and Salmén, L. (2004). "The softening behavior of hemicelluloses related to moisture," in: *Hemicelluloses: Science and Technology*, ACS Symposium Series 864, P. Gatenholm and M. Tenkanen (eds.), American Chemical Society, Washington, D.C., USA, pp. 184-197. https://doi.org/10.1021/bk-2004-0864.ch013

Pandey, K. K. (1999). "A study of chemical structure of soft and hardwood and wood polymers by FTIR spectroscopy," *Journal of Applied Polymer Science* 71(12), 1969-1975. https://doi.org/10.1002/(SICI)1097-4628(19990321)71:12%3C1969::AID-APP6%3E3.0.CO;2-D

Pettersen, R. C. (1984). "The chemical composition of wood," *Advances in Chemistry* 207, 57-126. https://doi.org/10.1021/ba-1984-0207.ch002

Poletto, M., Ornaghi Júnior, H. L., and Zattera, A. J. (2014). "Native cellulose: Structure, characterization and thermal properties," *Materials* 7(9), 6105-6119. https://doi.org/10.3390/ma7096105

Poletto, M., Zattera, A. J., and Santana, R. M. C. (2012). "Structural differences between wood species: Evidence from chemical composition, FTIR spectroscopy, and thermogravimetric analysis," *Journal of Applied Polymer Science* 126(S1), E337-E344. https://doi.org/10.1002/app.36991

Poletto, M., Zattera, A. J., Forte, M. M. C., and Santana, R. M. C. (2012a). "Thermal decomposition of wood: Influence of wood components and cellulose crystallite size," *Bioresource Technology* 109, 148-153. https://doi.org/10.1016/j.biortech.2011.11.122

Salmén, L. (1984). "Viscoelastic properties of *in situ* lignin under water-saturated conditions," *Journal of Materials Science* 19(9), 3090-3096.

Sun, N., Das, S., and Frazier, C. E. (2007). "Dynamic mechanical analysis of dry wood: Linear viscoelastic response region and effects of minor moisture changes," *Holzforschung* 61(1), 28-33. https://doi.org/10.1515/HF.2007.006

Traoré, M., Kaal, J., and Martínez Cortizas, A. (2018). "Differentiation between pine woods according to species and growing location using FTIR-ATR," *Wood Science and Technology* 52(2), 487-504. https://doi.org/10.1007/s00226-017-0967-9

Wang, T., Zhang, R., Peng, L., Ai, Y., and Lu, Q. (2017). "Pyrolysis characteristic changes of poplar wood during natural decay," *Journal of Analytical and Applied Pyrolysis*, 128, 257-260. https://doi.org/10.1016/j.jaap.2017.10.003

White, R. H., and Dietenberger, M. A. (2010). "Fire safety of wood construction," in: *Wood Handbook: Wood as an Engineering Material*, Ch. 18, USDA Forest Service,

Forest Products Laboratory. https://www.fpl.fs.usda.gov/documnts/fplgtr/fpl_gtr190.pdf

White, R. H., and Dietenberger, M. A. (2001). "Wood products: Thermal degradation and fire," in: *Encyclopedia of Materials, Science and Technology*, Elsevier Science Ltd., 9712-9716.

Žajdlík, T. and Šuhajda, K. (2022). "Experimental testing results of a timber structure's fire resistance in a combustion chamber," *Key Engineering Materials* 932, 225-230. https://doi.org/10.4028/p-r5a1b4

Article submitted: September 24, 2025; Peer review completed: December 13, 2025; Revised version received and accepted: January 2, 2026; Published: February 16, 2026.
DOI: 10.15376/biores.21.2. 3115-3136